# Surface Modification of CdS Nanoparticles with $MoS_4^{2-}$: A Case Study of Nanoparticle−Modifier Electronic Interaction

**David Diaz,[†,‡] Juvencio Robles,[§] Tong Ni,[†] Silvia-Elena Castillo-Blum,[‡] Datattri Nagesha,[†] Octavio-Jaime Alvarez-Fregoso,[⊥] and Nicholas A. Kotov*[,†]**

*Department of Chemistry and Center for Laser and Photonics Research, Oklahoma State University, Stillwater, Oklahoma 74078; Facultad de Quñmica, Universidad Nacional Autónoma de Mexico, Coyoacan, Mexico D.F., 04510 Mexico; Facultad de Quñmica, University of Guanajuato, Noria Alta s/n, Guanajuato GTO, 36050 Mexico; and Instituto de Investigacion en Materiales, Universidad Nacional Autónoma de Mexico, Coyoacan, Mexico D.F., 04510 Mexico*

*Received: June 24, 1999; In Final Form: September 13, 1999*

Modification with thiomolybdate results in the attachment of spatially separated $MoS_4^{2-}$ groups to the surface of CdS. This produces the red shift of excitonic absorption and emission bands and splitting of the trapped emission band. Because of the spatial gap between the thiomolybdate molecules of the modifying layer, the interaction of individual groups of the modifier with the CdS core must be considered. This was accomplished by using the density functional theory (DFT) description of a $MoS_4^{2-}$−CdS model cluster. Geometry, dipole moment, and localization of calculated molecular orbitals allow for the consistent description of optical effects observed for thiomolybdate-modified CdS nanoparticles, such as the red shift of adsorption and emission bands, enhancement of excitonic emission, and splitting of the trapped emission band. A good agreement between DFT calculated and experimental FTIR spectra has been obtained.

## I. Introduction

Surface modification of semiconductor nanoparticles (NP) is the primary means for tailoring their optical properties and 2D/3D organization.[1−5] Coating of NP with a different semiconducting material was shown to have a profound impact on the photophysics of the nanocrystalline core.[6−14] A broad range of intensities and spectral emission characteristics can be obtained by varying the thickness and the band gap ($E_g$) of the overlayer. Deposition of a semiconductor with a large $E_g$ relative to the core typically results in the enhancement of NP emission due to the suppression of radiationless recombination mediated by surface states[6−15] while the degree of charge carrier confinement does not change. Conversely, a layer from a small $E_g$ semiconductor provides additional area of delocalization for electron and hole.[10−17] The relaxation of the confinement regime results in the red shift of spectral features.

In the case of more abundant molecular organic modifiers, as opposed to semiconductor coatings, the extent of interaction between HOMO and LUMO of their electronic systems with VB and CB of the core is still poorly understood.[18] The solid-state approach employed for core−shell semiconductor systems[19−21] is not applicable for most of molecular modifiers since their surface layer cannot be described by using the band-gap concept. Therefore, the interaction of individual molecules with the core should be considered. Theoretically, to evaluate these interactions, semiempirical or *ab initio* theoretical descriptions of molecular systems should be employed, but their practical applicability is hampered by the complexity of the calculation requiring optimization of systems with thousands of atoms involved.

To better understand the electronic processes during the surface modification of nanoparticles and to find out the conditions that must be met for effective coupling between the electronic systems of the core and a molecular modifier, a simple model system should be utilized. As such, $MoS_4^{2-}$ ions were found to covalently bind to the surface of CdS nanoparticles, while retaining their identity. Unlike typical organic modifiers (thiols, amines, heterocycles, etc.), each thiomolybdate group effectively interacts with the *core* levels of the NP, which can be observed as a red shift of the excitonic absorption and emission peaks. Electronic processes between the core and the modifier were described by using density functional theory calculations of a small model cluster. The latter were shown to be an effective tool for analyzing the structure and electron-transfer processes on the surface of NP. A similar approach can be extended to other types of surface modification of semiconductor colloids and can be used in the design of a broad range of optical, catalytic, and electronic materials.

## II. Experimental Section

Preparation of DMSO dispersions of CdS nanoclusters stabilized by 2-ethylhexanoate was described elsewhere.[22]

UV−vis absorption spectra were taken by using HP8453 and HP8452A diode array Hewlett-Packard spectrophotometers. Fluorescence spectra were taken on a modular Fluorolog 3 SPEX spectrofluorometer. A 510 FTIR (7000−50 $cm^{-1}$) Nicolet instrument was used to take far-IR spectra. The samples for FTIR study were pressed in the form of pellets made of 10% semiconductor nanocrystalline samples mixed with 90% polyethylene powder.

High-resolution transmission electron microphotographs (HR-TEM) were obtained by using a JEOL 4000 Ex instrument operating at 400 kV. A 200 mesh copper grid was coated with a layer of carbon. A drop of DMSO dispersion was deposited onto Cu grids, and then the solvent was evaporated under vacuum.

[†] Oklahoma State University.
[‡] Facultad de Quñmica, Universidad Nacional Autónoma de Mexico.
[§] University of Guanajuato.
[⊥] Instituto de Investigacion en Materiales, Universidad Nacional Autónoma de Mexico.
* Corresponding author. E-mail kotov@okway.okstate.edu.

10.1021/jp992122n CCC: $18.00 
Published on Web 10/21/1999

*Ab initio* density functional theory calculations[23] were carried out on a Silicon Graphics Indigo-2 workstation (150 MHz, R4000 MIPS Processor, IRIX 6.2 operating system, 160 MB RAM, 5.0 GB disk). The level of theory and numerical accuracy attained for our all-electron full geometry optimizations without any symmetry restrictions is LSDA-VWN/DN(*)//LSDA-VWN/DN(*); i.e., all optimized geometries, wave functions, and energies were obtained employing the Vosko−Wilkes−Nusair local spin density functional[24] with a DN(*) polarized basis set, which yields a numerical accuracy comparable with the 6-31G-(*) basis set. For our calculations and visualizations we employed the Spartan V4.0 software package from Wavefunction, Irvine, CA.

The geometry optimization and molecular modeling of CdS tetrahedral clusters (Figures 6 and 7) were done by using the CAChe 3.11 (1998) software package from Oxford Molecular within MM/AM1, ZINDO, and PM3 approximations. Cd−S bond lengths were calculated to be 2.512, 2.488−2.491, and 2.480−2.492 Å for edges, (111) faces, and interior of the CdS tetrahedrons, respectively. Corresponding experimental values determined for thiol-modified clusters from X-ray diffraction patterns are 2.46−2.55 Å (edges) and 2.49−2.54 Å (faces and interior).[25,26]

## III. Results and Discussion

**III.1. Surface Modification by $MoS_4^{2-}$: Structure and Optical Properties.** Two stabilizers employed in the synthesis of 22.5 Å CdS nanoparticles, i.e., 2-ethylhexanoate anion (ethex) and DMSO, are relatively weakly bound to CdS yet provide nanoparticles with a sufficiently sharp size distribution. Such a synthetic procedure does not allow for the gradual variation of the particle diameter, which certainly is a drawback. On the other hand, the noncovalent binding of the stabilizers has also some advantages. The weak stabilization is significant for this work for two reasons. (1) The quantum mechanical model (see below) implies that the CdS surface is bare. The inclusion of covalently bound long-chain stabilizers (even in a clipped form) in calculations capable of predicting electron density distribution and molecular orbitals is difficult due to limitations on the number of atoms. The CdS surface with weakly bound surfactants matches the model of the "naked" cluster better than the one with a dense layer of covalently bound stabilizers. (2) The noncovalently bound stabilizer molecules do not compete with the surface modifier for the surface site, which allows for the modifier to bind in an optimal way. The latter is of particular importance for surface modifiers capable of forming more than one covalent bond with the CdS surface simultaneously such as thiomolybdate ion. The optimal geometry of binding, considered in the quantum mechanical model, is easier to achieve without the obstruction of strong stabilizers, that is, for relatively labile ionic surfactants.

After ripening, ethex/DMSO-stabilized CdS reveals a maximum of absorption at 365 ± 5 nm (3.4 ± 0.06 eV) and emission maximum at $\lambda_{max} = 402$ nm, $\Delta\lambda_{1/2} = 40$ nm (Figure 1a). TEM and XRD data indicate that CdS is formed in a cubic crystal lattice.[22] The high negative charge on tetrathiomolybdate ions, $MoS_4^{2-}$, makes them excellent electron-donating ligands with electron density being predominantly located on sulfur atoms. Therefore, a substantial change in optical characteristics of $MoS_4^{2-}$ upon reaction with NP can be expected. Indeed, in the UV−vis absorption spectrum, the reaction between CdS nanoparticles and $MoS_4^{2-}$ can be observed as a decrease of intensity of absorption of thiomolybdate at 321 and 473 nm (Figure 1b). Simultaneously, the peak of excitonic absorption of NP shifts to the red by 7 nm.

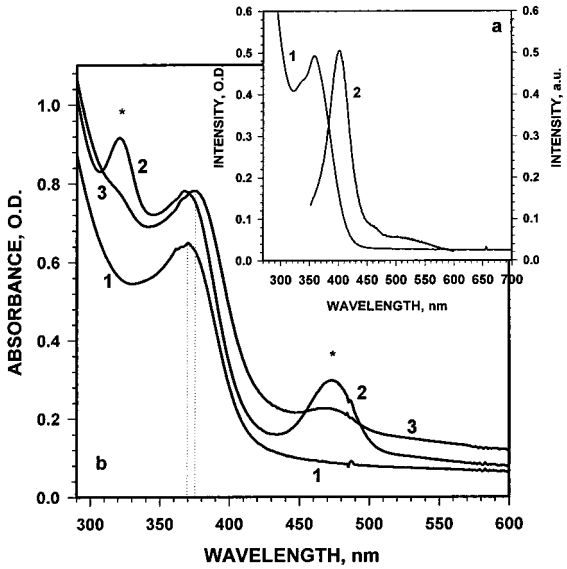


**Figure 1.** (a) UV−vis absorption (1) and emission (2) spectra of ripened CdS nanoparticles, $\lambda_{ex} = 340$ nm. (b) UV−vis absorption spectra of CdS nanoparticles (1), CdS nanoparticles immediately after mixing with $MoS_4^{2-}$ in a molecular ratio 250:1 $MoS_4^{2-}$ groups per nanoparticle (2), and in 30 min after mixing (3). Stars denote the characteristic peaks of $MoS_4^{2-}$ in DMSO.

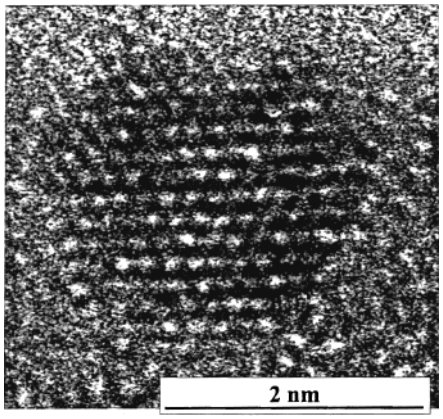


**Figure 2.** Transmission electron microscopy images of CdS nanoparticles after the modification in a molecular ratio of 150:1 $MoS_4^{2-}$ groups per nanoparticle.

From the decrease of intensity of absorption bands of $MoS_4^{2-}$ and absorption coefficients,[27,28] one can calculate an approximate number of groups attached to CdS nanocrystal. The surface area of CdS with $d = 22.5$ Å is 1590 Å$^2$. From the length of the Mo−S bond, e.g., 2.22 Å,[29,30] and the tetrahedral geometry of $MoS_4^{2-}$, a diameter of a $MoS_4^{2-}$ is estimated to be 2.6 Å, which corresponds to an approximate surface area required to accommodate one $MoS_4^{2-}$ unit of 6.7 Å$^2$. In a closely packed layer, about 240 $MoS_4^{2-}$ groups can be adsorbed on a single CdS particle. When the decrease of the 473 nm line of $MoS_4^{2-}$ levels off in ca. 30 min after the beginning of the reaction, 170 ± 20 molecules of $MoS_4^{2-}$ reacted per one CdS nanocluster. A large number of these groups are believed to deposit on the CdS surface, forming a shell with a submonolayer coverage; however, the photodecomposition of the thiomolybdate and its oxidation by traces of dissolved $O_2$ make some contribution to the total number of reacted $MoS_4^{2-}$, too.

The TEM image of CdS nanoparticles modified with $MoS_4^{2-}$ is virtually identical to those of nonmodified CdS (Figure 2 compared to Figure 3 in ref 22). This indicates that a thick continuous film of $MoS_2$ does not form. Importantly, there is

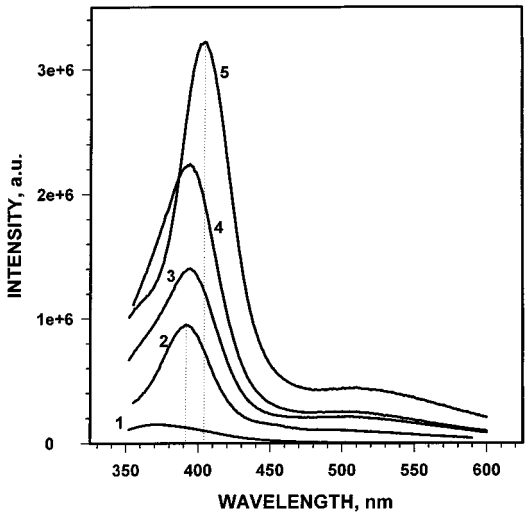


**Figure 3.** Luminescence spectra of $MoS_4^{2-}$ (1) and ripened CdS nanoparticles modified with $MoS_4^{2-}$ in a molecular ratio of 0:1 (2), 10:1 (3), 50:1 (4), and 100:1 (5) $MoS_4^{2-}$ units per nanoparticle; $\lambda_{ex} = 340$ nm.

no evidence of formation of large $MoS_2$ crystallites—individual or fused with CdS. Notably, the thinness of the $MoS_4^{2-}$ film on CdS and its discrete nature diminish the ability of the coating to diffract, which decreases its visibility in TEM pictures.

**Emission Spectra.** Two types of emission patterns can be observed for ethex/DMSO-stabilized CdS depending on the time of ripening. For fresh NP, the trapped emission at 490−505 nm dominates, but after a slow restructuring of NP, a near-band-gap excitonic line at 390−400 nm appears (Figures 1a and 3). The impact of $MoS_4^{2-}$ modification on the CdS emission differs significantly with respect to the type of prevalent luminescence.

The intensity of excitonic emission observed in the ripened dispersions increases for NP with thiomolybdate coating (Figure 3) and shifts by 15 nm to the red. Interestingly enough, while $MoS_4^{2-}$ can be considered as a monomer of $MoS_2$—a narrow-band-gap semiconductor with $E_g = 1.2$ eV[31,32]—the emission behavior after the modification appears to be the one intermediate between coatings with narrow- and wide-band-gap semiconductors. For instance, in HgS-coated CdS, the increase of the wavelength of the absorption onset occurs concomitantly with diminishing of the overall emission intensity of NP,[11,13,14,17,33,34] while the deposition of a wide-band-gap semiconductor enhances the excitonic emission, but virtually no change in the energy of emitted photons is observed.[6−9,15] For $MoS_4^{2-}$ modification, the stronger excitonic emission is accompanied by the bathochromic spectral shift in both absorption and emission. The elevated quantum yield of the excitonic emission indicates partial elimination of intra-band-gap electronic levels stimulating radiationless recombination. Since thiomolybdates are strong nucleophiles, filling the surface levels acting as electron traps can be suggested as the mechanism of emission enhancement.[35,36]

The red shift of the excitonic emission, 15 nm, is comparable to that of the absorption spectrum, which is 7 nm (Figure 1). The discrepancy between these two shifts is quite substantial and cannot be dismissed as an experimental error. Indeed, while being correlated to each other, the transformation of absorption and emission spectra upon modification, which perturbs the electronic structure of the core, should be most certainly quite distinct because the states responsible for "excitonic peaks" in absorption and emission differ are different for both CdSe NP[37] and tetrahedral CdS clusters.[38,39]

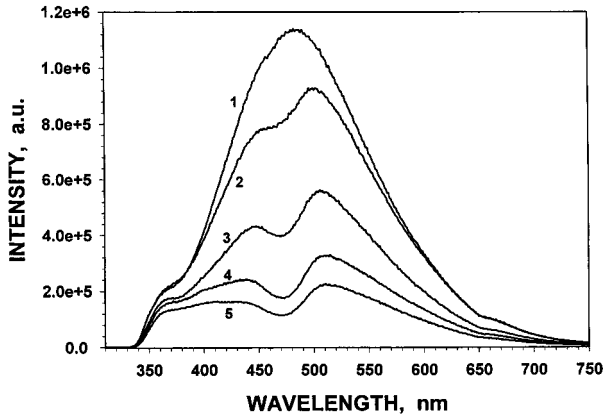


**Figure 4.** Luminescence spectra of fresh CdS nanoparticles modified with $MoS_4^{2-}$ in a molecular ratio of 0:1 (1), 12:1 (2), 25:1 (3), 50:1 (4), and 100:1 (5) $MoS_4^{2-}$ units per nanoparticle; $\lambda_{ex} = 300$ nm.

For freshly prepared CdS, charge carriers become quickly trapped in surface states and exhibit only a broad 490 nm band (Figure 4). The modification with $MoS_4^{2-}$ splits it into two peaks located at 437 and 505 nm. The integral intensity of trapped emission decreases, which is the combined outcome of the gradual filling of surface states and the inner filter effect. The positions of maxima of these peaks do not depend on the surface coverage by thiomolybdate units. This indicates that the observed emitting states at 437 and 505 nm on the modified surface have a localized character. Structurally, they may represent (1) new levels formed as a result of the modification and (2) preexisting charge carrier traps (see below).

**Infrared Spectra**. The far-infrared region, 50−800 $cm^{-1}$, is characteristic for vibrations associated with the semiconductor core. Raman scattering lines have been normally used to observe the longitudinal optical phonons (LO)[40−42] while IR spectra are typically employed to monitor covalent bonds in the organic shell of NP.[43−48] Partially, this is associated with the complexity of IR spectra in this region (Figure 5b). On the basis of literature data, the attribution of only a few peaks can be suggested. The low-energy vibrations from 80 to 190 $cm^{-1}$ have been ascribed to Cd−S bonds on and near the cluster surface.[25,49−51] As well, a correlation between the frequency of $\nu$(Cd−S) stretching vibrations in the core located from 245 to 290 $cm^{-1}$ and the diameter of NP has been observed.[49] Notably, this assignment is in contradiction with EXAFS results,[52] which revealed expansion of the Cd−S distance in thiol-capped CdS clusters with decreasing NP diameter due to the strain on the crystal lattice imposed by covalently bound thiols. Conversely, the reported IR data[49] suggest higher Cd−S vibrational frequencies for smaller clusters, which is indicative of shorter bonds.

Free $MoS_4^{2-}$ has a very broad peak at about 450 $cm^{-1}$, corresponding to a normal symmetric mode of tetrahedral molecules[53,54] broadened by an anisotropic environment in amorphous solid. Upon adsorption to CdS, two strong new bands at 320 and 340 $cm^{-1}$ appear, accompanied by four sharp peaks between 600 and 700 $cm^{-1}$. The nature of some of these vibrations is considered below. Now, it is significant to point out that $MoS_4^{2-}$ in the adsorbed state exhibits a few sharp FTIR peaks, rather than a featureless broad band. This suggests that the variations of geometry of attached $MoS_4$ units are small, and they exist in a distinct molecular environment rather than producing a variety of adsorbed states and conformations, which should result in inhomogeneously broadened IR bands as seen in Figure 5a,b.

**III.2. Electronic Effects of Surface Modification.** To some extent, the decrease of excitonic energy in the CdS/$MoS_4^{2-}$

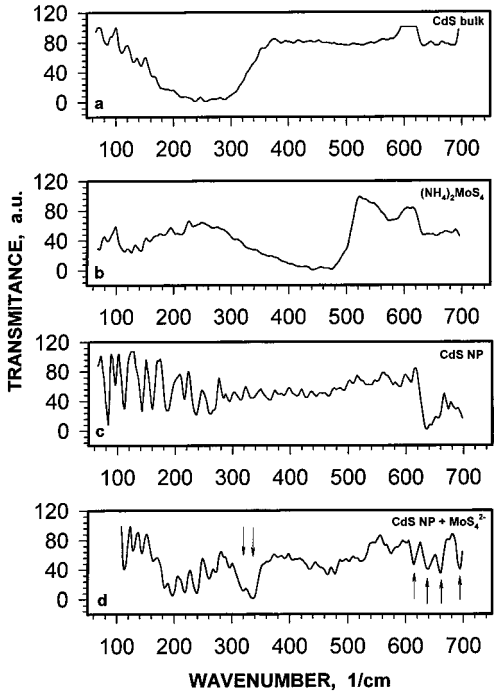


**Figure 5.** FTIR spectra of bulk CdS (a), $(NH_4)_2MoS_4$ (b), ethex-stabilized CdS nanoparticle (c), and CdS nanoparticles modified with $MoS_4^{2-}$ in a molecular ratio of 150:1 thiomolybdate units per nanoparticle (d). Arrows show the peaks characteristic for $MoS_4^{2-}$-modified CdS: 320, 340, 615, 638, 660, and 695 $cm^{-1}$.

system is reminiscent of the core−shell nanoparticles of CdS coated with small band-gap semiconductors.[10−13,55] However, the effective mass approximation or similar solid-state approach[10,13,17,55] is not applicable in the case of $MoS_4^{2-}$ modification. The discrete nature of the $MoS_2$ film does not allow for the analogy of hybrid semiconductor systems to be utilized here.[56] Therefore, a different approach to the description of the electronic interaction between the $MoS_4^{2-}$ overlayer and nanoparticles should be found. Such a description should include a concept of the electronic interaction of the surface modifier with the CdS core and should make provisions that individual $MoS_4^{2-}$ units are electronically fairly independent of each other due to physical separation of their adsorption sites.

A small fragment of the CdS surface with an attached $MoS_4^{2-}$ group of 15−20 atoms total can be taken as a model. For an atomic structure of this size, electronic states can be calculated by using both semiempirical and *ab initio* molecular modeling strategies. The resulting molecular orbitals can be treated as localized electronic states of the modified nanoparticle. From their energy, positioning, and morphology one may judge about their interaction with the core levels.

Prior to choosing the structure of the model cluster, it is necessary to consider how $MoS_4^{2-}$ is bound to CdS. The metal atoms on Cd-terminated faces of CdS are hexagonally packed and therefore provide geometrically matching adsorption sites for tetrahedral $MoS_4^{2-}$ molecules (Figures 6a and 7a). The gaps between Cd atoms on the (111) surface and the corresponding interatomic distance between covalently bound sulfur atoms, $d_{S-S}$, is 4.15 Å, which is somewhat larger than $d_{S-S}$ in $MoS_4^{2-}$ equal to 3.61 Å. A better match can be found for defect sites characteristic for excess of $Cd^{2+}$. The optimized S−S distances for adatoms of cadmium and sulfur vacancies (Figure 6b,c) are smaller than for perfect zinc blende CdS and are equal to 3.83−3.84 Å, which is closer to the natural $d_{S-S}$ in thiomolybdate. Therefore, smaller strain induced by binding to these defect points as well as their higher energy should lead to slightly more

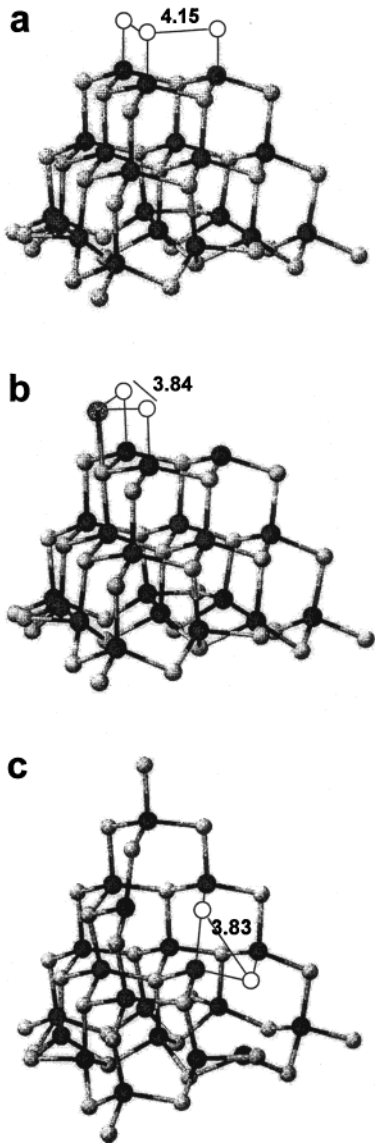


**Figure 6.** Adsorption sites for $MoS_4^{2-}$ on zinc blende CdS clusters. (a) Truncated CdS tetrahedron with exposed Cd-terminated (111) lattice plane. (b) An adsorption site provided by a cadmium adatom on the edge of a truncated tetrahedron. (c) An adsorption site provided by sulfur vacancies on a tetrahedral face. Light and dark dots indicate sulfur and cadmium atoms, respectively. Empty circles denote possible location of sulfur atoms. All distances are given in angstroms.

preferential binding of thiomolybdate to these sites than to (111) Cd-terminated faces.

Molecular modeling indicates that the lowest energy is attained when three out of four sulfur atoms of adsorbed $MoS_4^{2-}$ are fused with the CdS crystal lattice (Figure 7a,b). This remains valid for all types of adsorption sites, including the Cd-terminated surface of zinc blende CdS (Figure 7a), adatoms (Figure 7b, 1), and vacancies (Figure 7b, 2). On the basis of these results, the model cluster for DFT calculations can be selected. For the evaluation of electronic interactions, the surface of $MoS_4^{2-}$-modified CdS is modeled as a basic cubic unit consisting of three Cd and eight S atoms, from which four of the chalcogen atoms originate in the crystal lattice of the nanoparticle (Figure 8a, Table 1). The model cluster bears a close resemblance to the structure of thiomolybdate units on the CdS surface obtained by the molecular modeling (Figure 7), while the Cd dangling bonds are terminated with S−H groups. This is the smallest possible model cluster suitable for the description of covalent modification of the CdS surface by

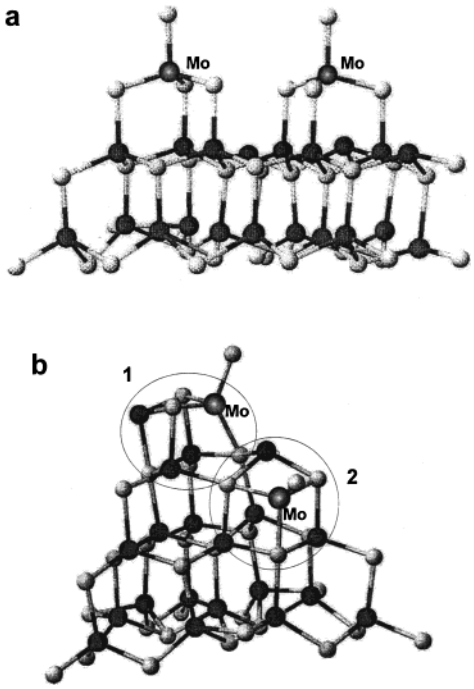


**Figure 7.** Optimized binding of $MoS_4^{2-}$ to (a) Cd-terminated (111) face and (b) to surface defects such as cadmium adatoms and sulfur vacancies. Circled areas 1 and 2 correspond to the structures obtained by reaction of $MoS_4^{2-}$ to tetrahedrons b and c in Figure 6. Light and dark dots correspond to sulfur and cadmium atoms, respectively.

thiomolybdate. While the quantum mechanical description of fragments including larger pieces of the CdS crystal lattice is a subject of our current work, the minimization of cluster size is necessary at this point to alleviate the computational cost problem associated with a large number of atoms.

**UV-vis Spectra.** Once the structure of the model cluster has been established, the DFT algorithm of quantum mechanical calculations can provide various information about the electronic processes at the surface and the interaction of the electronic systems of the modifier and nanoparticle. In particular, the shift of electron density can be assessed from the dipole moment, $\mu$. As expected from the strong nucleophilic character of $MoS_4^{2-}$, the modification results in a strong displacement of electron density from thiomolybdate group to CdS with calculated $\mu$ attaining a magnitude as high as 3.0 D, which can be used as a quantitative description of filling of the charge carrier traps (surface states) by electron donors seen as the enhancement of the excitonic emission.

The shift of electron density acquires additional tonality when considered in conjunction with the type of molecular orbitals forming during the modification. The primary contribution to the HOMO is made by the 3p orbitals of sulfur which belongs to the CdS crystal lattice. This finding is essential for the understanding of the observed optical effects. Because of the fact that the valence band (VB) of CdS is also formed from the same 3p orbitals of sulfur,[4,57,59] the HOMO of the model structure in Figure 8b will be virtually "dissolved" in the VB, thereby providing effective coupling of the core level and that of the modifier, $MoS_4^{2-}$. Taking into account that binding of thiomolybdate is associated with a considerable shift of electron density to the local HOMO, the surface modification should also give rise to the electron density inside the core. Because of the low degree of geometrical anisotropy of the NP, the dipole moment of CdS NP as a whole is unlikely to change significantly unless the binding is very limited and site specific, which cannot be justified in the $MoS_4^{2-}$ case (Figure 7). However,

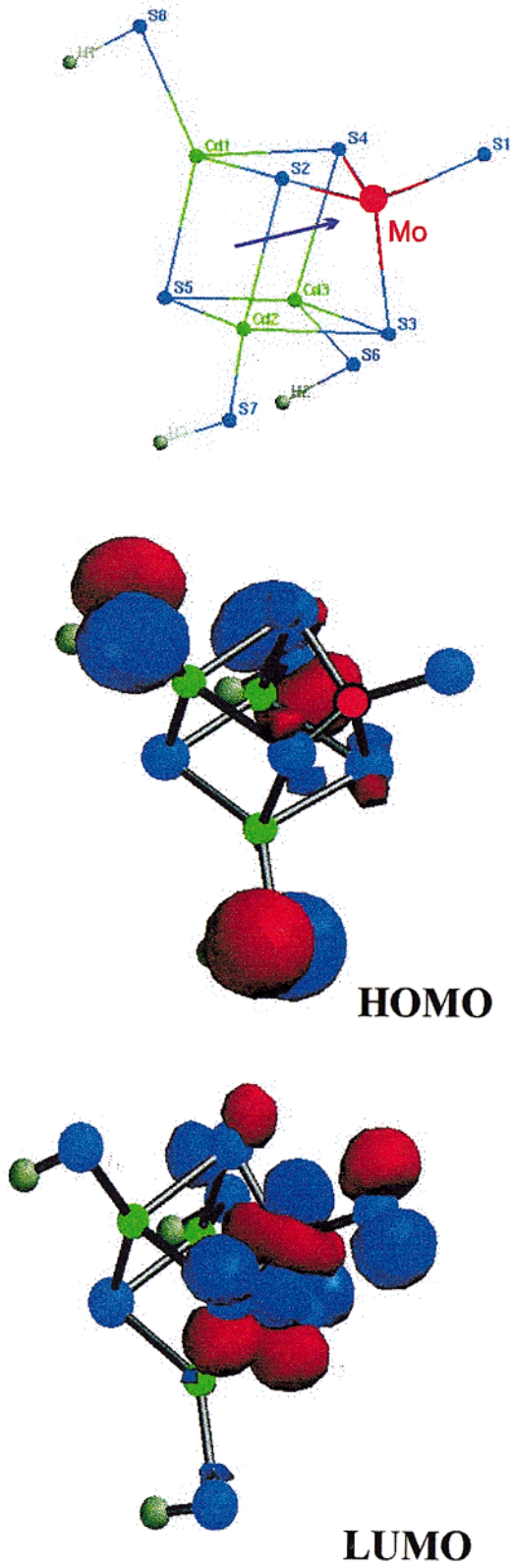


**Figure 8.** DFT calculations of a model CdS−$MoS_4^{2-}$ cluster: optimized geometry and dipole moment (a), HOMO (b), and LUMO (c). Sulfur, cadmium, and hydrogen atoms are denoted as blue, green, and gray dots, respectively. The molybdenum atom is represented as a bright red dot. The distances between atoms are given in Table 1.

the displacement of electrons during the modification should give rise to the electron density inside the core. This strengthens the Coulomb attraction between charge carriers in the excited state, which effectively reduces the energy of the first excitonic state.[4,19,57,59] Therefore, the bathochromic shift of the absorption

**TABLE 1: Interatomic Distances (in Å) of the Model Clusters**

| | calculated | | | calculated | |
|---|---|---|---|---|---|
| atoms | modified | non-modified[a] | atoms | modified | non-modified[a] |
| Cd1−S2 | 2.7147 | 2.6165 | Cd2−Cd3 | 3.4312 | 3.3166 |
| S2−Mo | 2.2435 | | Cd1−S5 | 2.5022 | 2.6206 |
| Cd1−Cd2 | 3.4338 | 3.3525 | Cd1−S8 | 2.4017 | 2.6539 |
| Cd1−Cd3 | 3.3988 | 3.3296 | | | |

[a] A nonmodified model cluster is obtained by the replacement of the Mo atom in Figure 8 with an atom of Cd and adding a capping H-atom to the $S^-$ terminus.

and emission maxima may be rationalized as the effect of increased electron density on the valence band inside the core. Note that an increase of electron density on the *conduction band* of the core would have resulted in partial band filling and a blue shift of spectral features known as the Burstein shift for doped bulk semiconductors and semiconducting electrodes.[58] Such an effect is unlikely to occur in modified nanoparticles, because this would require very high electron donor activity of the modifier, which will compromise its chemical stability in solutions.

The coupling of $MoS_4^{2-}$ and CdS electronic levels through 3p orbitals of sulfur suggests that the area of delocalization available for charge carriers of the core in the ground state is expanded. In other words, this can be described as mixing of electronic levels of the NP and those of the modifier. In unison with the increase of electron density, this should result in the red shift of optical features observed experimentally. At the moment, it is impossible to distinguish these two effects, which are equally important for the understanding of the perturbation of electronic structure of the core caused by surface modification.

The LUMO of the model cluster (Figure 8c) has a large contribution of 5d orbitals of the molybdenum atom and 3p orbitals of sulfur atoms originating from $MoS_4^{2-}$. Since LUMO of the model cluster does not incorporate 5s atomic orbitals of Cd atoms forming the conduction band (CB) of CdS, the coupling between these two states should be more complicated and will greatly depend on the energy gap between them.[60] In general, it should be more localized than the HOMO of the model cluster and therefore can be considered as a surface state in the $MoS_4^{2-}$-modified nanoparticle.

Considering the processes of optical excitation of a CdS nanoparticle, one may initially assume that the new electronic level described by the LUMO of the model cluster is located below the CB of the nanoparticle core. In this case, the transfer of electron density to the thiomolybdate ligand and entrapment of charge carriers in the localized states similar to LUMO of the model cluster should ensue the photoexcitation of the modified NP. After that, the evolution of this surface-localized excited state may include radiative recombination, radiationless decay, and thermal detrapping to the first excitonic level. At first sight, it would be quite logical to assign one of the new emission bands in Figure 4 to the radiative recombination on $MoS_4$ moieties. In this case, however, it is difficult to explain why the intensity ratio between the two peaks is virtually independent of the amount of $MoS_4^{2-}$ added: the relative height of a $MoS_4^{2-}$-induced emission must go up with the surface density of thiomolybdate groups. Simultaneously, such a new emission band should have been also visible in Figure 3 as a satellite of the excitonic emission for ripened NP.

As an alternative, one may consider that LUMO level of the $MoS_4^{2-}$- modified CdS is positioned above the CB of the core.

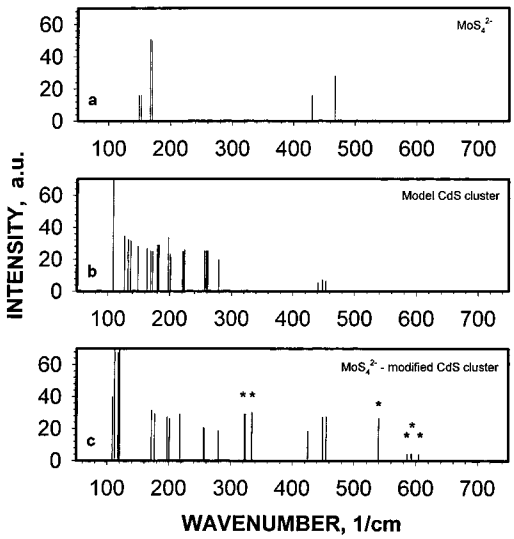


**Figure 9.** DFT calculations of FTIR absorption spectra of $MoS_4^{2-}$ (a), model CdS cluster (b), and $MoS_4^{2-}$-modified CdS cluster (c). The stars denote the FTIR peaks which are unique for the $MoS_4^{2-}$-modified surface.

In this case, the modification is likely to quench rather than to induce the trapped emission, since this will effectively reduce the number of intra-band-gap states participating in the radiative process. Taking into account the fact that the trapped emission band in CdS is a superposition of photons originating from a relatively large variety of recombination processes, the splitting of the trapped emission peak can be described as the elimination of a particular type of surface traps by raising their energy above the CB, while the others remain active and retain their characteristics. Structurally, they can be represented by the defects that provide favorable conditions for $MoS_4^{2-}$ binding, such as the ones presented in Figure 6, and the ones that do not. Those remaining after the modification of the intra-band-gap states may be, for instance, buried sulfur vacancies and/or sulfur adatoms on [111] faces. As one can see in Figure 4, the relative position of the minimum at 475 nm becomes deeper and deeper as the modification progresses, which corresponds to the energy of the surface defects that were deactivated by the surface modification. For this model, the ratio between the peaks becomes a function of a relative abundance of different types of traps set by the synthetic procedure. Therefore, it is unaffected by $MoS_4^{2-}$ and is independent of its amount.

For ripened nanoparticles with the near-band-gap luminescence, the elevation of the energy of the defect sites above the bottom of CB after their reaction with $MoS_4^{2-}$ manifests as the enhancement of the excitonic emission (Figure 3). This effect is a natural consequence of reduction of the number of the surface states stimulating radiationless transitions from the lowest excitonic state.

**IR Spectra.** By using the DFT algorithm, the model $MoS_4^{2-}$−CdS cluster, analogous CdS cluster, and $MoS_4^{2-}$ ion corresponding FTIR spectra can be calculated (Figure 9). The theoretical spectrum of the model cluster confirms the assignments of experimentally observed peaks in the 100−200 $cm^{-1}$ range to the surface atoms of CdS nanoclusters;[51] however, it provides a different interpretation for the 245−290 $cm^{-1}$ peaks seen in IR as the vibrations unrelated to the Cd−S stretch in the core. The calculated lines within these limits are located at 258, 261, and 278 $cm^{-1}$. They represent symmetric and asymmetric breathing modes of the CdS model cluster resulting in the concerted elongation of several surface Cd−S bonds. The energy of these vibrations is dependent on the type and surface

density of the stabilizer, curvature of the NP surface, and therefore on the size of the clusters. For the modified NP, all the peaks that distinguish the calculated spectrum of these species from the both original components can be found in the experimental spectrum. The two strong bands at 320 and 340 $cm^{-1}$ appearing only after the modification (Figure 5d) find an excellent match in the calculated spectrum. The corresponding theoretical lines of the model cluster are positioned at 324 (double degenerate) and 334 $cm^{-1}$ (Figure 9c) and exhibit almost equal intensity. These modes correspond to concerted stretches of CdS bonds in the model cluster, which become IR-active (i.e., associated with the change in dipole moment) due to the change of the electron density distribution on the surface upon $MoS_4^{2-}$ modification. Taking into account the simplicity of the model cluster, the overall likeness between the experimental and theoretical IR spectra is quite remarkable. To some extent, this can be attributed to the structural similarity between the weakly stabilized CdS NP approaching the state of the bare CdS surface and the model used for the FTIR calculations.

## IV. Conclusion

Modification of CdS with thiomolybdate anion, $MoS_4^{2-}$, results in the red shift of absorption and emission excitonic peaks and splitting of the trapped emission band, which indicates the presence of effective electronic interaction of the modifier with the surface states and the core states of NP. To understand the mechanism of the electronic processes upon covalent binding of a discrete molecules to CdS, the electronic effects of $MoS_4^{2-}$ modification must be described on the basis of the electronic interaction of individual thiomolybdate groups with the CdS lattice. Molecular orbital calculations by using the density functional theory are found to be a useful tool for this purpose. They demonstrate a strong shift of electronic density from $MoS_4^{2-}$ to the CdS core, which decreases the energy of the first excitonic state. The involvement of the 3p AO orbitals of sulfur atoms incorporated in the CdS crystal lattice suggests strong coupling of the HOMO of the model cluster to the valence band in CdS core, which results in an expansion of the delocalization volume of the charge carriers. The red shift of absorption features is rationalized as the combined product of both the electron density displacement and the HOMO−VB conjugation.

Similar processes produce the red shift of the excitonic luminescence band. However, the LUMO of the model cluster does not include the 5s AO orbitals of Cd atoms being quite distant from each other on the energy scale (ref 60). Therefore, the coupling of this energy level and the CB is less likely.

Splitting of the trapped emission band is attributed to quenching of a particular type of surface defects resulting from molecularly selective binding of the thiomolybdate group. Specificity of binding is associated with the formation of two covalent bonds demanding optimal geometrical positioning of the Cd atoms on the surface of the nanoparticle. This distinguishes $MoS_4^{2-}$ from the most common types of surface modifiers such as thiols, amines, and heterocycles. Interestingly enough, the experimental and DFT-calculated FTIR spectra of the modified nanoparticles are found to be in a good agreement, which permitted determination of the vibrational modes of the observed FTIR bands.

Overall, the analysis of electronic interactions presented here is expected to be applicable to other types of surface modifiers, where interactions of individual molecular groups with the semiconductor core need to be considered.

**Acknowledgment.** This work was supported by NSF CAREER award, NSF-EPSCoR, Energy Research Center, and OSU Sensor Center (N.A.K.). Funds for the 400 and 600 MHz NMR spectrometers for the Oklahoma Statewide Shared NMR facility were provided by the National Science Foundation (Grant BIR-9512269), the Oklahoma State Regents for Higher Education, the W. W. Keck Foundation, and Conoco Inc. The generosity of Alexander von Humboldt Stiftung is gratefully acknowledged. N.A.K. thanks all members of the Hamburg group (Dr. H. Weller) for stimulating discussions. This work was also partially supported by CONACyT (Projects 400313-5-1016P to D.D. and 25059-E to J.R.). D.D. expresses his gratitude to the Fullbrigth-Garcia-Robles Foundation and to DGAPA-UNAM (Project IN100398) for the financial support. We also thank Luis Redon from IFUNAM for the HR-TEM images. D.D. and J.R. are grateful to Guillermo Mendoza for useful comments.

## References and Notes

(1) Alivisatos, A. P. *J. Phys. Chem.* **1996**, *100*, 13226. Peng, X.; Wilson, T. E.; Alivisatos, A. P.; Schultz, P. G. *Angew. Chem., Int. Ed. Engl.* **1997**, *36 (1/2)*, 145−147.

(2) Beecroft, L. L.; Ober, C. K. *Chem. Mater.* **1997**, *9*, 1302−1317.

(3) Herron, N.; Thorn, D. L. *Adv. Mater.* **1998**, *10*, 1173−1184.

(4) Woggon, U. *Optical Properties of Semiconductor Quantum Dots*; Springer-Verlag: Berlin, 1997.

(5) Vossmeyer, T.; Jia, S.; Delonno, E.; Diehl, M. R.; Kim, S. H.; Peng, X.; Alivisatos, A. P.; Heath, J. R. *J. Appl. Phys.* **1998**, *84*, 3664−3670.

(6) Dabbousi, B. O.; Rodriguez-Viejo, J.; Mikulec, F. V.; Heine, J. R.; Mattoussi, H.; Ober, R.; Jensen, K. F.; Bawendi, M. G. *J. Phys. Chem. B* **1997**, *101*, 9463−9475.

(7) Danek, M.; Jensen, K. F.; Murray, C. B.; Bawendi, M. G. *Chem. Mater.* **1996**, *8*, 173.

(8) Peng, X.; Schlamp, M. C.; Kadavanich, A. V.; Alivisatos, A. P. *J. Am. Chem. Soc.* **1997**, *119*, 7019−7029.

(9) Hines, M. A.; Guyot-Sionnest, P. *J. Phys. Chem.* **1996**, *100*, 468.

(10) Eychmuller, A.; Hasselbarth, A.; Weller, H. *J. Lumin.* **1992**, *53*, 113.

(11) Hasselbarth, A.; Eychmuller, A.; Eichberger, R.; Giersig, M.; Mews, A.; Weller, H. *J. Phys. Chem.* **1993**, *97*, 5333−5340.

(12) Kamalov, V. F.; Little, R.; Logunov, S. L.; El-Sayed, M. A. *J. Chem. Phys.* **1996**, *100*, 6381.

(13) Zhou, H. S.; Sasahara, H.; Homma, I.; Komiyama, H.; Haus, J. *Chem. Mater.* **1994**, *6*, 1534−1541.

(14) Alivisatos, A. P. *Science* **1996**, *271*, 933−941.

(15) Counio, G.; Esnouf, S.; Gacoin, T.; Boilot, J. P. *J. Phys. Chem.* **1996**, *100*, 20021−20026.

(16) Han, M. Y.; Huang, W.; Chew, C. H.; Gan, L. M.; Zhang, X. J.; Ji, W. *J. Phys. Chem. B* **1998**, *102*, 1884−1887.

(17) Tian, Y. C.; Newton, T.; Kotov, N. A.; Guldi, D. M.; Fendler, J. H. *J. Phys. Chem.* **1996**, *100*, 8927−8939.

(18) In small particles, the valence and conduction bands split into separate electronic levels. The top of the valence band becomes HOMO, while the bottom of the conduction band can be considered as LUMO of the nanocluster. Nevertheless, VB and CB notations are used here in order to underscore the origin of these molecular orbitals and to avoid possible confusion with HOMO and LUMO of the modifier.

(19) Brus, L. E. *J. Chem. Phys.* **1984**, *80*, 4403−4409.

(20) Fojtik, A.; Weller, H.; Koch, U.; Henglein, A. *Ber. Bunsen-Ges. Phys. Chem.* **1984**, *88*, 969.

(21) Chestnoy, N.; Hull, R.; Brus, L. E. *J. Chem. Phys.* **1986**, *85*, 2237.

(22) Diaz, D.; Rivera, M.; Ni, T.; Castillo-Blum, S.-E.; Rodriguez, J.-C.; Nagesha, D.; Robles, J.; Alvarez- Fregoso, A.-F.; Kotov, N. *J. Phys. Chem. B* **1999**, *103*, 9854.

(23) Parr, R. G.; Yang, W. *Density Functional Theory of Atoms and Molecules*; Oxford University Press: New York, 1989.

(24) Vosko, S. H.; Wilk, L.; Nusair, M. *Can. J. Phys.* **1980**, *58*, 1200.

(25) Dance, I. G.; Choy, A.; Scudder, M. L. *J. Am. Chem. Soc.* **1984**, *106*, 6285−6295.

(26) Vossmeyer, T.; Reck, G.; Schultz, B.; Katsikas, L.; Weller, H. *J. Am. Chem. Soc.* **1995**, *117*, 12881.

(27) Muller, A.; Diemann, E.; Jostes, R.; Bogge, H. *Angew. Chem., Int. Ed. Engl.* **1981**, *20*, 934−955.

(28) Wilcoxon, J. P.; Samara, G. A. *Phys. Rev.* **1995**, *51*, 7299−7302.

(29) Greany, M. A.; Coyle, C. L.; Harmer, M. A.; Jordan, A.; Stiefel, E. I. *Inorg. Chem.* **1989**, *28*, 919−920.

(30) Beqqali, O. El.; Zorkani, I.; Rogemond, F.; Chermette, H.; Chaabane, R. B.; Gamoudi, M.; Guillard, G. *Synth. Met.* **1997**, *90*, 165−172.
(31) Parsapour, F.; Kelley, D. F.; Craft, S.; Wilcoxon, J. P. *J. Chem. Phys.* **1996**, *104*, 4978−4987.
(32) Pouzet, J.; Hadouda, H.; Bernede, J. C.; Le Ny, R. *J. Phys. Chem. Solids* **1998**, *57*, 1363−1369.
(33) Banin, U.; Mews. A.; Kadavanich, A. V.; Guzelian, A. A.; Alivisatos, A. P. *Mol. Cryst. Liq. Cryst. A* **1996**, *283*, 1−10.
(34) Schooss, D.; Mews, A.; Eychmuller, A.; Weller, H. *Phys. Rev. B* **1994**, *49*, 17072−17078.
(35) Chandler, R. R.; Coffer, J. L. *J. Phys. Chem.* **1991**, *95*, 4−6.
(36) Dannhauser, T.; O'Neil, M.; Johanson, K.; Whitten, D.; McLendon, G. *J. Phys. Chem.* **1986**, *90*, 6074.
(37) Norris, D. J.; Bawendi, M. G. *J. Chem. Phys.* **1995**, *103*, 5260−5267.
(38) Herron, N.; Calabrese, J. C.; Farneth, W. E.; Wang, Y. *Science* **1993**, *259*, 1426.
(39) Hasselbarth, A.; Eychmuller, A.; Weller, H. *Chem. Phys. Lett.* **1993**, *203*.
(40) Colvin, V. L.; Goldstein, A. N.; Alivisatos, A. P. *J. Am. Chem. Soc.* **1992**, *114*, 5221−5230.
(41) Shiang, J. J.; Kadavanich, A. V.; Grubbs, R. K.; Alivisatos, A. P. *J. Phys. Chem.* **1995**, *99*, 17417.
(42) Zou, S.; Weaver, M. J. *J. Phys. Chem.* **1999**, *103*, 2323−2326.
(43) Bowen, K.; Colvin, V. L.; Alivisatos, A. P. *J. Phys. Chem.* **1994**, *98*, 4109.
(44) Deng, H. H.; Li, M.; Zhang, Y.; Lu, Z. H.; Fu, D. G. *Chem. Lett.* **1997**, 483−484.
(45) Gard, R.; Sun, Z.-X.; Forsling, W. *J. Colloid Interface Sci.* **1995**, *169*, 393−399.
(46) Majetich, S. A.; Carter, A. C. *J. Phys. Chem.* **1993**, *97*, 8727.
(47) Trindade, T.; O'Brien, P.; Zhang, X. M. *Chem. Mater.* **1997**, *9*, 523−530.
(48) Veinot, J. G.; Ginzburg, M.; Pietro, W. J. *Chem. Mater.* **1997**, *9*, 2117−2122.
(49) Lover, T.; Bowmaker, G. A.; Seakins, J. M.; Cooney, R. P. *Chem. Mater.* **1997**, *9*, 967−975.
(50) Lover, T.; Bowmaker, G. A.; Seakins, J. M.; Cooney, R. P.; Henderson, W. *J. Mater. Chem.* **1997**, *7*, 647−651.
(51) Melendres, C. A.; Bowmaker, G. A.; Leger, J. M.; Beden, B. *J. Electroanal. Chem.* **1998**, *449*, 215−218.
(52) Rockenberger, J.; Troger, L.; Kornowski, A.; Vossmeyer, T.; Eychmuller, A.; Feldhaus, J.; Weller, H. *J. Phys. Chem. B* **1997**, *101*, 2691−2701.
(53) Ferraro, J. R. *Low-frequency Vibrations of Inorganic and Coordination Compounds*; Plenum Press: New York, 1971; p 247.
(54) Nakamoto, K. *Infrared and Raman Spectra of Inorganic and Coordination Compounds*, 3rd ed.*;* Wiley: New York, 1978; p 132.
(55) Mews, A.; Banin, U.; Kadavanich, A. V.; Alivisatos, A. P. *Ber. Bunsen.-Ges. Phys. Chem.* **1997**, *101*, 1621−1625.
(56) Calculations of the level structure of CdS nanoparticles modified by $MoS_4^{2-}$ were performed by using the software developed by D. Schoos et al. in ref 34. In these calculations, the layer of the modifier was approximated by a layer of $MoS_2$ with $E_g = 1.2$ eV. For a 3.1 Å shell of $MoS_2$, which would correspond to a unit cell of molybdenum sulfide, a theoretically predicted shift of the absorption spectrum should be between 0.41 and 0.58 eV, which is much bigger that the observed value of 0.075 eV. The authors thank A. Mews for the help with the software.
(57) Brus, L. E. *Isr. J. Chem.* **1993**, *33*, 9−13.
(58) Fitzmaurice, D. *Sol. Energy Mater. Sol. Cells* **1994**, *32*, 289−305. Amalnerkar, D. P.; Yamaguchi, K.; Kajita, T.; Minoura, H. *Solid State Commun.* **1994**, *90*, 3−6.
(59) Rosenblit, M.; Jortner, J. *J. Phys. Chem.* **1994**, *98*, 9365−9370.
(60) The positions of HOMO and LUMO of the model cluster in energy scale in respect to the energy of electron in vacuum were calculated to be −0.1055 eV (triple degenerate) and −0.0594 eV (double degenerate), respectively. The positions of the top of VB and the bottom of CB in a 19 Å CdS cluster were reported to be at −0.2 and 2.5 eV, respectively (Hill, N. A.; Whalley, K. B. *J. Chem. Phys.* **1993**, *99*, 3707−3715). Theoretically, these values of energy for HOMO and VB are close enough while those of LUMO and CB are too far apart for the delocalization to occur. Although both of these facts are in accord with the optical data, low accuracy of electronic level energy calculations and difficulties in accounting for the solvent effect make such comparison of state energies in two species problematic.